Morphological Control of ZnO Nanostructures by Electrodeposition

Lifen Xu,[†] Yi Guo,[†] Qing Liao,[‡] Jianping Zhang,[‡] and Dongsheng Xu*,[†]

State Key Laboratory for Structural Chemistry of Unstable and Stable Species, College of Chemistry and Molecular Engineering, Peking University, Beijing 100871, P. R. China, and Institute of Chemistry, Chinese Academy of Science, Beijing 100080, P. R. China

Received: February 27, 2005; In Final Form: May 19, 2005

We report here an electrodeposition route for the preparation of oriented and well-defined ZnO nanostructures by kinetically controlling the growth rates of various facets of the deposit by appropriate capping agents. We demonstrated that adsorption of Cl^- takes places preferentially onto the (0001) planes to hinder the crystal growth along the *c*-axis, and results in the formation of platelet-like crystals. It is also shown that the morphology evolved from hexagonal tapers to hexagonal rods and rhombohedral rods by changing the compositions of the capping agents. Furthermore, strong UV emissions at 380∼390 nm and negligible green bands at around 500 nm were observed, indicating that these ZnO electrodeposits are highly crystallized and of excellent optical quality.

Introduction

The synthesis of inorganic nanostructures with well-defined shapes has attracted extraordinary attention due to the importance of the dimensionality of materials in determining their properties.[1] Solution-phase synthetic approaches have been applied with a high degree of success to produce a variety of nanocrystal materials with special morphologies.[2−7] In these strategies, the presence of chemically dissimilar lattice faces can be selectively bound by capping reagents to change the growth kinetics and surface energies of different crystal faces, which can ultimately lead to anisotropic growth of low-symmetry nanostructures. Electrodeposition in solutions presents a cost-effective method for preparation of large area thin films, in terms of its low-temperature processing, arbitrary substrate shapes, and precise control of the film thickness. Although the role of strongly adsorbed species in controlling the size and even shape of the deposits has been realized in electroplating,[8,9] the direct electrochemical growth of nanostructures with controlled crystalline morphology is still not well exploited.

ZnO is an important semiconducting oxide with a wide band gap for smart devices and optoelectronics.[10] Well-defined ZnO nanostructures, such as rods, columns, platelets, and complex column-to-rod bilayers, have recently been synthesized via hydrothermal solution processes.[11−14] Electrodeposition of ZnO films has been demonstrated by several groups,[15−19] and has been used in creating oriented arrays of ZnO nanorods and flat disklike deposits.[17−19] Our strategy to control the shape and the orientation of crystallites consists of electrodepositing ZnO thin films directly onto indium-doped tin oxide (ITO) covered glass substrates and adding low molecular mass or salts as shape-control agents. Novel well-defined ZnO nano-/microstructures such as hexagonal nanotapers, hexagonal platelets, and rhombohedral rods were formed by using simple amine and inorganic ions to control the growth behavior of the crystal.

* Author to whom correspondence should be addressed. E-mail: dsxu@pku.edu.cn. Phone: 86-10-62753580. Fax: 86-10-62751725.

[†] Peking University.

[‡] Chinese Academy of Science.

Experimental Section

Thin films of ZnO were electrodeposited in 0.05 M $Zn(NO_3)_2$ aqueous solutions using the method developed by Izaki and Omi.[15] To control the shapes, several kinds of amine and inorganic salts such as KCl, NH_4F, CH_3COONH_4, and ethylenediamine (EDA) were added to the zinc nitrate baths. The ITO glass substrate with a sheet resistance of about 20 Ω/□ was cleaned ultrasonically in 0.1 M NaOH, distilled water, and acetone and then rinsed in distilled water again. All depositions were carried out in a configured glass cell at 70 °C, in which an ITO substrate, a platinum plate, and a saturated calomel electrode (SCE) served as the working electrode, counter electrode, and reference electrode, respectively. All electrodepositions were done at a potential of −1.10 V vs SCE. The durations of the depositions were 1.5 h.

The morphology and the phase indentification of the products were characterized by field-emission scanning electron microscopy (SEM) (Strata DB235 FIB) and power X-ray diffractometry (D/MAX-PC 2500 with Cu Kα radiation and a normal $\theta-2\theta$ scan), respectively. Further structural analysis of individual ZnO microstructure was carried out using transmission electron microscopy (TEM) (JEOL 200CX TEM). Room-temperature photoluminescent (PL) spectra of the films deposited on ITO were measured using a pulsed Nd:YAG laser (266 nm) as an excitation source with energy in the range of millijoules.

Results and Discussion

Figure 1a shows the SEM image of the ZnO films electrodeposited from 0.05 M $Zn(NO_3)_2$ solution. It can be seen that well-aligned single-crystalline hexagonal particles typically 0.5 μm in diameter are grown along the ⟨0001⟩ direction perpendicularly onto the substrates. Panels b and c of Figure 1 show the SEM images of the ZnO platelets electrodeposited by addition of 0.06 M KCl. These platelets are 10 μm in diameter and 70−400 nm in thickness. The electron diffraction pattern from one sheet (Figure 1c) can be indexed as a hexagonal wurtzite structure recorded along the ⟨0001⟩ zone, further confirming that it is a single crystal. In addition, we note that addition of 0.05 M CH_3COONH_4 also yields platelet-like crystals.

10.1021/jp051007b CCC: $30.25
Published on Web 06/24/2005

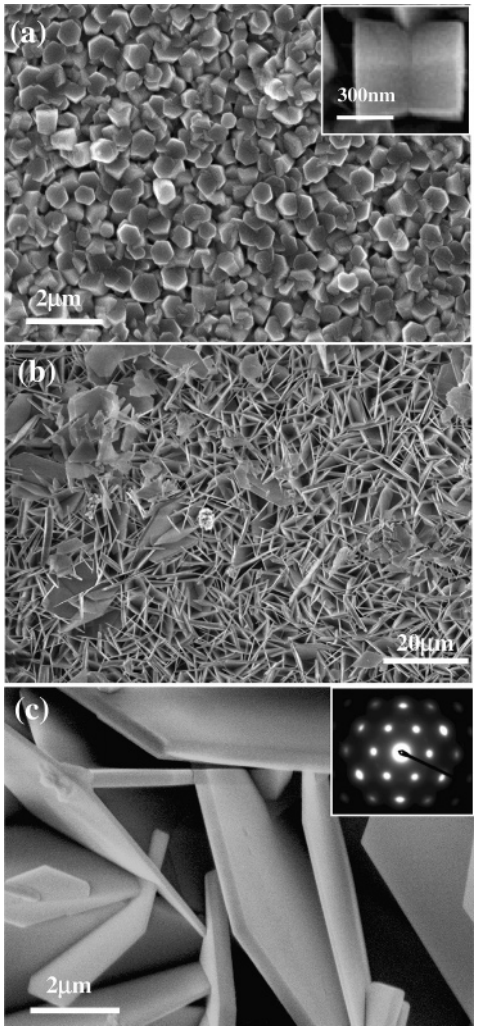

Figure 1. SEM images of the ZnO nanostructures by electrodeposition from solutions containing (a) 0.05 M $Zn(NO_3)_2$ and (b, c) 0.05 M $Zn(NO_3)_2$ + 0.06 M KCl. Inset in Figure 1c is an electron diffraction pattern recorded on the platelet along the ⟨0001⟩ zone.

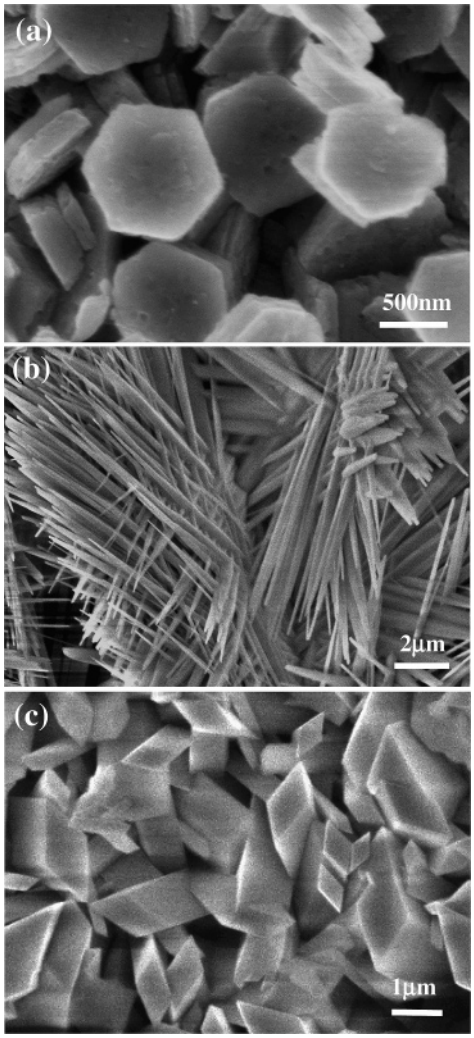

Figure 2. SEM images of the ZnO nanostructures by electrodeposition from solutions containing 0.05 M $Zn(NO_3)_2$ and NH_4F with different concentrations: (a) 9 mM, (b) 0.02 M, and (c) 0.2 M.

Figure 2 displays typical ZnO crystals grown on the ITO glass surfaces at different NH_4F concentrations. When a very small quantity of NH_4F was added, the hexagonal particles became thinner and larger for the (0001) faces (Figure 2a). Further additions of NH_4F caused the formation of woven ZnO nanorods with needlelike branches (Figure 2b). The root size of the needles varied between 50 and 300 nm. The average length of these needles was around 10 μm, and each needle had a very sharp tip. It is noted that the roots of the needles are not in a hexagonal form. ZnO rods with the rhombohedral morphology are obtained at a much higher NH_4F concentration (Figure 2c). The widths of these rhombohedral rods are in the range of 0.2−1 μm and the length-to-width ratios are about 2 to 10. A further increase of the NH_4F concentration does not change the rhombohedral morphology of ZnO, but does decrease the length-to-width ratios.

Panels a−c of Figure 3 display typical ZnO crystals grown on the ITO substrates with EDA added in the solution. The dosage of EDA is controlled until the solution turns clear. In this case, homogeneous taper-like nanostructures several square centimeters in area are routinely obtained. These deposits look like hexagonal tapers, about 2 μm in height and 100−500 nm in diameter at their base. Figure 3d gives a typical transmission electron microscopy (TEM) image of an individual hexagonal taper, indicating that the diameters of the rods are gradually decreased from the root to form a sharp tip. The electron diffraction pattern (the inset in Figure 2d) shows ⟨0001⟩ as the growth direction for the nanotaper.

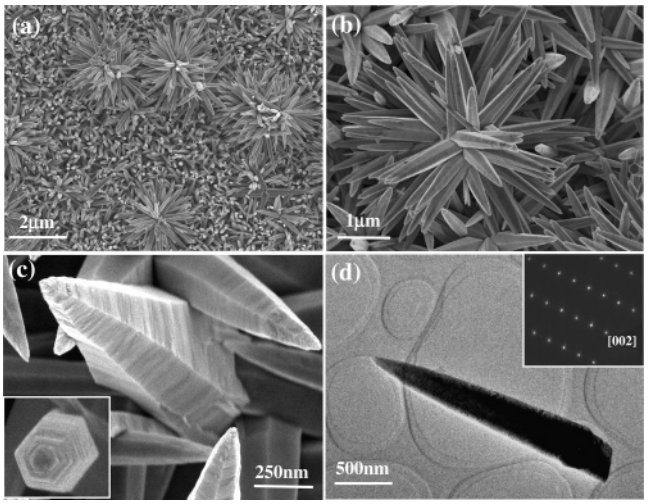

Figure 3. (a−c) SEM and (d) TEM images of the ZnO nanostructures by electrodeposition from solutions containing 0.05 M $Zn(NO_3)_2$ and 0.013 M EDA. The inset in part d is an electron diffraction pattern corresponding to the ⟨001⟩ zone axis of a ZnO single nanotaper.

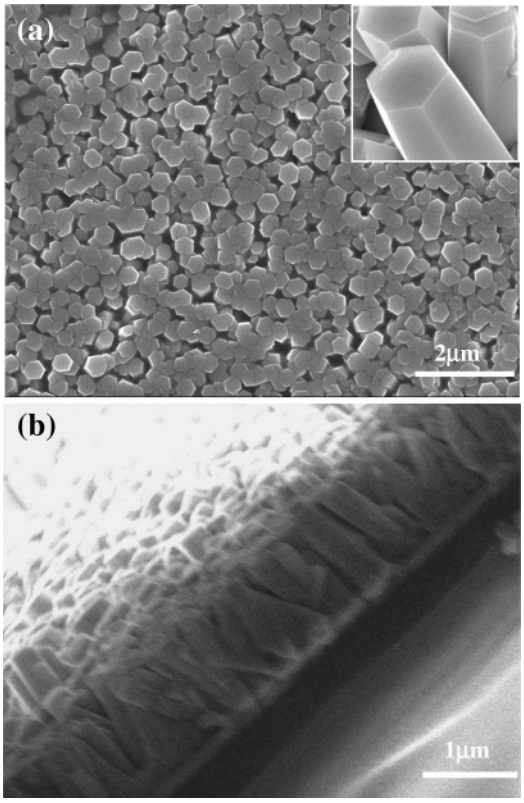

Figure 4. SEM images of the ZnO nanostructures by electrodeposition from solutions containing 0.05 M $Zn(NO_3)_2$ and 0.06 M KCl and 0.01 M EDA: (a) top view and (b) side view.

Furthermore, the control deposition experiment, from a solution containing 0.05 M $Zn(NO_3)_2$, 0.06 M KCl, and 0.01 M EDA, yielded hexagonal ZnO rods (Figure 4a). These rods are 100−300 nm in diameter and tightly arranged. The cross-sectional image (Figure 4b) indicated that the nanorods are uniform in lengths of about 2 μm and vertically aligned on the ITO substrate. In addition, we further found that the aspect ratio of the rods becomes lower with an increase in the concentration of KCl or a decrease in the concentration of EDA.

Figure 5 shows the XRD patterns of electrodeposited ZnO films with different morphologies. All of the XRD patterns can be indexed as hexagonal wurtzite structures of ZnO. From these XRD data, we can illustrate the texture effect of the anisotropic morphology and orientation on the relative intensity of the diffraction peak (normalized to the ⟨101⟩ line, which usually corresponds to the maximum intensity of ZnO). As expected, a substantially higher intensity is observed for the ⟨002⟩ diffraction peaks in the XRD patterns of the hexagonal particle films (Figure 5a) and the highly aligned nanorod arrays (Figure 5d), indicating that the ZnO crystallites are oriented perfectly with their *c*-axis being perpendicular to the ITO substrates. For the taper-shaped thin film, corresponding to the sample in Figure 3, its XRD pattern (Figure 5c) also presents a preferential ⟨001⟩ orientation, but the intensities of the (100) and (101) diffraction peaks slightly increase, as compared to those of the the pure particle film (Figure 5a). From the XRD pattern of the sheet-shaped deposits (Figure 5b), it is found that the (100) diffraction peak is largely enhanced at the expense of the (002) peak.

It is clear from the above observations that the morphologies of the electrodeposited ZnO evolved from mesoparticles to platelets and nanorods with adding different capping agents. Previous studies also show the shape control of the electrodeposits varying the reduction potentials.[9] They interpreted the shape formation using a model that minimizes the total surface

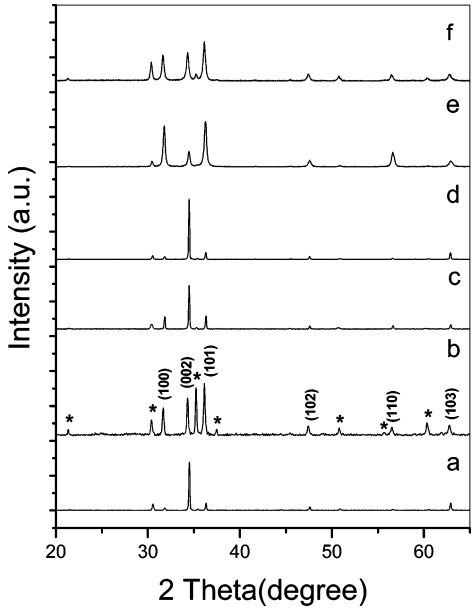

Figure 5. XRD patterns of the ZnO nanostructures with different morphologies: (a) hexagonal particles; (b) hexagonal platelets; (c) hexagonal tapers; (d) hexagonal rod arrays; (e) woven nanoneedles; and (f) rhombohedral rods. An asterisk indicates the ITO substrate.

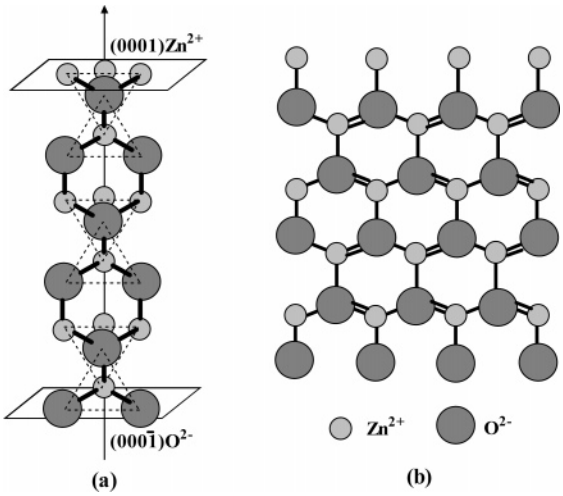

Figure 6. Crystalline structure of the wurtzite structured ZnO (a) along the ⟨0001⟩ direction and (b) { 10$\bar{1}$0} face.

and twin-boundary energies of an assembly of single-crystal units at constant volume. However, in our approach, the applied potentials and the concentrations of $Zn(NO_3)_2$ are constant for all of the electrodeposition. In colloidal synthesis, it is well-known that some capping molecules can block certain faces and enhance growth of other facets. Here, we also believe that the capping effect plays a key role for anisotropic growth of various ZnO nanostructures.

ZnO has a wurtzite structure that is described as a number of alternating planes composed of 4-fold coordinated O^{2-} and Zn^{2+} ions, stacked alternatively along the *c* axis, as shown in Figure 6a. The typical crystal habit exhibits a basal polar oxygen plane (000$\bar{1}$), a top tetrahedron corner-exposed polar zinc plane (0001), and low-index faces (parallel to the *c*-axis) consisting of a nonpolar {10$\bar{1}$0} face (Figure 6b). It can be suggested that negative ions in the solution are adsorbed on the positive polar face of (0001) by electrostatic force, which allows the anisotropic growth of the crystal along the ⟨0001⟩ direction. In the early stages of the electrodeposition, $Zn(OH)_4^{2-}$ ions, the growing unit in the solution near the surface of the ZnO crystal,

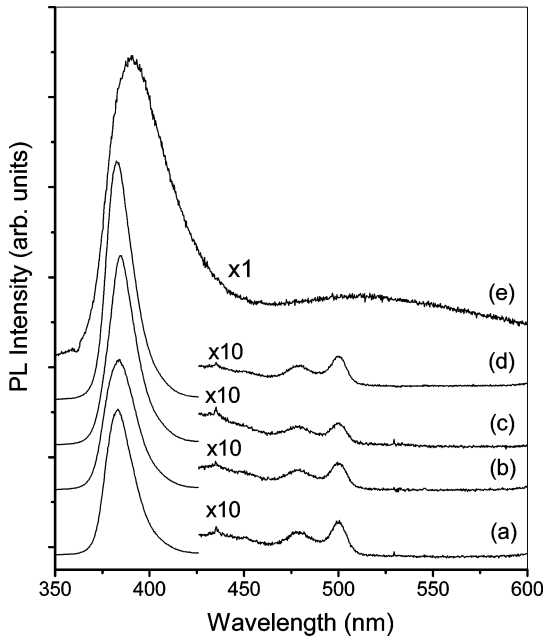

Figure 7. Room-temperature PL spectra from the ZnO thin films of (a) hexagonal particles as shown in Figure 1a, (b) hexagonal tapers as shown in Figure 3, (c) hexagonal platelets as shown in Figure 1b, (d) hexagonal rod arrays as shown in Figure 4, and (e) rhombohedral rods as shown in Figure 2c.

are likely adsorbed on the positive polar face of the (0001) surface, resulting in faster growth along the ⟨0001⟩ direction. When we added large amounts of KCl or CH_3COONH_4 into the solution, Cl^- or CH_3COO^- ions would be adsorbed preferentially on the positive polar face of the (0001) surface, which prevented the contact of $Zn(OH)_4^{2-}$ on the (0001) surface and thus limited the crystal growth along the *c*-axis (Figure 1b,c). In the case of adding the neutral EDA molecule, the electrostatic force between the positive polar face of (0001) and the negative $Zn(OH)_4^{2-}$ growth unit is much stronger than the adsorption affinity between the neutral EDA molecule and the (0001) face. Therefore, adsorption of the EDA molecule and $Zn(OH)_4^{2-}$ would occur on the lateral $\{10\bar{1}0\}$ surfaces group and the (0001) face, respectively. The growth along the side direction may be largely limited due to the strong coordination ability of EDA to zinc, and the crystal growth rate along the ⟨0001⟩ direction is enhanced. As a result, the (0001) face contracts and even disappears to form a hexagonal taper shape (Figure 3). Furthermore, by blocking simultaneously both EDA and Cl^- on the lateral $\{0\bar{1}10\}$ surfaces group and the (0001) face, the contract rate of the (0001) face decreases, yielding hexagonal ZnO rods (Figure 4). The formation mechanisms for rhombohedral particles are still under investigation. This may also be attributed to selective binding of NH_3 or F^-, which in turn changes surface energies of different crystal faces and hence the growth kinetics there.

The PL properties of various ZnO nanostructures obtained by electrodeposition were measured by using a pulsed Nd:YAG laser (266 nm in wavelength, several millijoules in power) as an excitation source. All samples for PL measurements were preannealed at 400 °C in N_2 for 1 h. Figure 7 gives the room-temperature PL spectra recorded from the ZnO thin films with different morphologies. The dominant peaks at ∼383 nm are observed in all ZnO samples with hexagonal morphologies (curves a−d), which can be attributed to free-exciton. Two weak deep level emissions at 480 and 500 nm are due to impurities and native defects, such as interstitial zinc atoms in the ZnO crystal.[18,20] The green band at around 500 nm related to oxygen vacancy is almost negligible, indicating that these ZnO electrodeposits are highly crystallized and of excellent optical quality. It is interesting that the peak positions of the free-exciton peaks red shift from ∼383 to ∼390 nm when the shapes evolve from hexagonal structures to woven nanoneedles (curves f).

Conclusion

In summary, we report here an electrodeposition route for the preparation of well-defined ZnO nanostructures by kinetically controlling the growth rates of various facets of the deposit with appropriate capping agents. It is demonstrated that adsorption of Cl^- or CH_3COO^- takes places preferentially onto the (0001) plane to produce platelet-like crystals, in contrast to the needlelike structures obtained by addition of EDA or NH_4F. It is also shown that the morphology evolved from hexagonal rods to woven nanoneedles and rhombohedral rods by changing the compositions of the mixed capping agents. Importantly, this electrodeposition approach may provide a versatile and facile pathway for designing nano-/mesostructures with novel morphologies.

Acknowledgment. This work is supported by NSFC (Grant No. 20433010) and MSTC (MSBRDP, Grant No. 2000077503).

References and Notes

(1) (a) Alivisatos, A. P. *J. Phys. Chem.* **1996**, *100*, 13226. (b) Hu, J.; Odom, T. W.; Lieber, C. M. *Acc. Chem. Res.* **1999**, *32*, 435. (c) Xia, Y.; Yang, P.; Sun, Y.; Wu, Y.; Mayers, B.; Gates, B.; Yin, Y.; Kim, F.; Yan, Y. *Adv. Mater.* **2003**, *15*, 353. (d) Pan, Z. W.; Dai, Z. R.; Wang, Z. L. *Science* **2001**, *291*, 1947. (e) Xu, D. S.; Xu, Y. J.; Chen, D. P.; Guo, G. L.; Gui, L. L.; Tang, Y. Q. *Adv. Mater.* **2000**, *12*, 520.

(2) (a) Peng, X.; Manna, L.; Yang, W.; Wickham, J.; Scher, E.; Kadavanich, A.; Alivisatos, A. P. *Nature* **2000**, *404*, 59. (b) Manna, L.; Scher, E. C.; Alivisatos, A. P. *J. Am. Chem. Soc.* **2000**, *122*, 12700.

(3) Wang, X.; Li, Y. *J. Am. Chem. Soc.* **2002**, *124*, 2880.

(4) (a) Chen, M.; Xie, Y.; Lu, J.; Xiong, Y. J.; Zhang, S. Y.; Qian, Y. T.; Liu, X. M. *J. Mater. Chem.* **2002**, *12*, 748. (b) Yan, P.; Xie, Y.; Wang, W.; Liu, F.; Qian, Y. T. *J. Am. Chem. Soc.* **1999**, *121*, 4062.

(5) Sun, Y.; Xia, Y. *Science* **2002**, *298*, 2176.

(6) Lu, Q.; Gao, F.; Zhao, D. *Angew, Chem., Int. Ed.* **2002**, *41*, 1932.

(7) Qi, L. M.; Cölfen, H.; Antonietti, M. *Angew. Chem., Int. Ed.* **2000**, *39*, 604.

(8) Mastai, Y.; Gal, D.; Hodes, G. *J. Electrochem. Soc.* **2000**, *147*, 1435.

(9) Xiao, Z. L.; Han, C. Y.; Kwok, W. K.; Wang, H. H.; Welp, U.; Wang, J.; Crabtree, G. W. *J. Am. Chem. Soc.* **2004**, *126*, 2316.

(10) (a) Bagnall, D. M.; Chen, Y. F.; Zhu, Z.; Yao, T.; Koyama, S.; Shen, M. Y.; Goto, T. *Appl. Phys. Lett.* **1997**, *70*, 2230. (b) Cao, H.; Xu, J. Y.; Zhang, D. Z.; Chang, S.-H.; Ho, S. T.; Seelig, E. W.; Liu, X.; Chang, R. P. H. *Phys. Rev. Lett.* **2000**, *84*, 5584. (c) Huang, M. H.; Mao, S.; Feick, H. N.; Yan, H. Q.; Wu, Y. Y.; Kind, H.; Weber, E.; Russo, R.; Yang, P. D. *Science* **2001**, *292*, 1897.

(11) (a) Tian, Z. R.; Voigt, J. A.; Liu, J.; Mckenzie, B.; Mcdermott, M. J. *J. Am. Chem. Soc.* **2002**, *124*, 12954. (b) Tian, Z. R.; Voigt, J. A.; Liu, J.; Mckenzie, B.; Mcdermott, M. J.; Rodriguez, M. A.; Konishi, H.; Xu, H. F. *Nature Mater.* **2003**, *2*, 821.

(12) (a) Vayssieres, L.; Keis, K.; Lindquist, S. E.; Hagfeldt, A. *J. Phys. Chem. B* **2001**, *105*, 3350. (b) Vayssieres, L.; Keis, K.; Hagfeldt, A.; Lindquist, S. E. *Chem. Mater.* **2001**, *13*, 4395. (c) Vayssieres, L. *Adv. Mater.* **2003**, *15*, 464.

(13) Greene, L. E.; Law, M.; Goldberger, J.; Kim, F.; Johnson, J. C.; Zhang, Y. F.; Saykally, R. J.; Yang, P. D. *Angew. Chem., Int. Ed.* **2003**, *42*, 3031.

(14) Zhang, J.; Sun, L. D.; Liao, C. S.; Yan, C. H. *Chem. Commun.* **2002**, 262.

(15) Izaki, M.; Omi, T. *Appl. Phys. Lett.* **1996**, *68*, 2439.

(16) Peulon, S.; Lincot, D. *J. Electrochem. Soc.* **1998**, *145*, 864.

(17) Liu, R.; Vertegel, A. A.; Bohannan, E. W.; Sorenson, T. A.; Switzer, J. A. *Chem. Mater.* **2001**, *13*, 508.

(18) Vanheusden, K.; Warren, W. L.; Seager, C. H.; Tallant, D. R.; Voigt, J. A.; Gnade, B. E. *J. Appl. Phys.* **1996**, *79*, 7983.

(19) (a) Yshida, T.; Tochimoto, M.; Schlettwein, D.; Wöhrle, D.; Sugiura, T.; Minoura, H. *Chem. Mater.* **1999**, *11*, 2657. (b) Yshida, T.; Minoura, H. *Adv. Mater.* **2000**, *12*, 1219.

(20) Li, Y.; Cheng, G. S.; Zhang, L. D. *J. Mater. Res.* **2000**, *15*, 2305.